

Alma Mater Studiorum Università di Bologna  
Archivio istituzionale della ricerca

The inhibition of gadolinium ion (Gd<sup>3+</sup>) on the mitochondrial F<sub>1</sub>FO-ATPase is linked to the modulation of the mitochondrial permeability transition pore

This is the final peer-reviewed author's accepted manuscript (postprint) of the following publication:

*Published Version:*

Algieri, C., Trombetti, F., Pagliarani, A., Fabbri, M., Nesci, S. (2021). The inhibition of gadolinium ion (Gd<sup>3+</sup>) on the mitochondrial F<sub>1</sub>FO-ATPase is linked to the modulation of the mitochondrial permeability transition pore. INTERNATIONAL JOURNAL OF BIOLOGICAL MACROMOLECULES, 184, 250-258 [10.1016/j.ijbiomac.2021.06.065].

*Availability:*

This version is available at: <https://hdl.handle.net/11585/826671> since: 2021-09-06

*Published:*

DOI: <http://doi.org/10.1016/j.ijbiomac.2021.06.065>

*Terms of use:*

Some rights reserved. The terms and conditions for the reuse of this version of the manuscript are specified in the publishing policy. For all terms of use and more information see the publisher's website.

This item was downloaded from IRIS Università di Bologna (<https://cris.unibo.it/>).  
When citing, please refer to the published version.

(Article begins on next page)

This is the final peer-reviewed accepted manuscript of:

**The inhibition of gadolinium ion (Gd<sup>3+</sup>) on the mitochondrial F1FO-ATPase is linked to the modulation of the mitochondrial permeability transition pore.**

**Algieri C, Trombetti F, Pagliarani A, Fabbri M, Nesci S. Int J Biol Macromol. 2021 Jun 11;184:250-258.**

The final published version is available online at:  
<https://doi.org/10.1016/j.ijbiomac.2021.06.065>

Rights / License:

The terms and conditions for the reuse of this version of the manuscript are specified in the publishing policy. For all terms of use and more information see the publisher's website.

*This item was downloaded from IRIS Università di Bologna (<https://cris.unibo.it/>)*

***When citing, please refer to the published version.***

The inhibition of gadolinium ion ( $Gd^{3+}$ ) on the mitochondrial  $F_1F_0$ -ATPase is linked to the modulation of the mitochondrial permeability transition pore

Cristina Algieri, Fabiana Trombetti, Alessandra Pagliarani\*, Micaela Fabbri, Salvatore Nesci\*

Department of Veterinary Medical Sciences (DIMEVET), University of Bologna, via Tolara di Sopra, 50, 40064 Ozzano Emilia (Bologna), Italy.

\*Corresponding authors: [alessandra.pagliarani@unibo.it](mailto:alessandra.pagliarani@unibo.it) (AP); [salvatore.nesci@unibo.it](mailto:salvatore.nesci@unibo.it) (SN)

Keywords: gadolinium ion; mitochondria;  $F_1F_0$ -ATPase; permeability transition pore; metal cofactors; enzyme kinetics.

## Abstract

The mitochondrial permeability transition pore (PTP), which drives regulated cell death when  $\text{Ca}^{2+}$  concentration suddenly increases in mitochondria, was related to changes in the  $\text{Ca}^{2+}$ -activated  $\text{F}_1\text{F}_0$ -ATPase. The effects of the gadolinium cation ( $\text{Gd}^{3+}$ ), widely used for diagnosis and therapy, and reported as PTP blocker, were evaluated on the  $\text{F}_1\text{F}_0$ -ATPase activated by  $\text{Mg}^{2+}$  or  $\text{Ca}^{2+}$  and on the PTP.  $\text{Gd}^{3+}$  more effectively inhibits the  $\text{Ca}^{2+}$ -activated  $\text{F}_1\text{F}_0$ -ATPase than the  $\text{Mg}^{2+}$ -activated  $\text{F}_1\text{F}_0$ -ATPase by a mixed-type inhibition on the former and by uncompetitive mechanism on the latter. Most likely  $\text{Gd}^{3+}$  binding to  $\text{F}_1$ , is favoured by  $\text{Ca}^{2+}$  insertion. The maximal inactivation rates ( $K_{\text{inact}}$ ) of pseudo-first order inactivation are similar either when the  $\text{F}_1\text{F}_0$ -ATPase is activated by  $\text{Ca}^{2+}$  or by  $\text{Mg}^{2+}$ . The half-maximal inactivator concentrations ( $K_i$ ) are  $2.35 \pm 0.35$  mM and  $0.72 \pm 0.11$  mM, respectively. The potency of a mechanism-based inhibitor ( $K_{\text{inact}}/K_i$ ) also highlights a higher inhibition efficiency of  $\text{Gd}^{3+}$  on the  $\text{Ca}^{2+}$ -activated  $\text{F}_1\text{F}_0$ -ATPase ( $0.59 \pm 0.09 \text{ mM}^{-1} \cdot \text{s}^{-1}$ ) than on the  $\text{Mg}^{2+}$ -activated  $\text{F}_1\text{F}_0$ -ATPase ( $0.13 \pm 0.02 \text{ mM}^{-1} \cdot \text{s}^{-1}$ ). Consistently, the PTP is desensitized in presence of  $\text{Gd}^{3+}$ . The  $\text{Gd}^{3+}$  inhibition on both the mitochondrial  $\text{Ca}^{2+}$ -activated  $\text{F}_1\text{F}_0$ -ATPase and the PTP strengthens the link between the PTP and the  $\text{F}_1\text{F}_0$ -ATPase when activated by  $\text{Ca}^{2+}$  and provides insights on the biological effects of  $\text{Gd}^{3+}$ .

## 1. Introduction

The  $F_1F_0$ -ATPase, an oligomeric complex of the inner mitochondrial membrane (IMM) ubiquitous in mammals, is an energy-transducing machine characterized by a reversible working mode of ATP synthesis/hydrolysis [1]. According to the chemiosmotic theory, the  $H^+$  transfer from the mitochondrial matrix to the intermembrane space by the respiratory complexes, pushed by substrate oxidation, creates the protonmotive force ( $\Delta p$ ) that is converted into a useful chemical form, ATP [2]. Contrary, in the reverse-mode, the hydrolysis of the high-energy phosphoanhydridic bonds of ATP drives  $H^+$  pumping in the intermembrane space and energizes the IMM. The bi-functional catalysis of the  $F_1F_0$ -ATPase is a unique energy transmission mechanism sustained by the structural enzyme arrangement in two molecular motors, a hydrolytic  $F_1$  sector and a hydrophobic  $F_0$  sector. The two sectors are coupled by a reversible torque generation [3,4] (Fig. 1). The catalytic domain  $F_1$  is a globular hexamer in which three  $\alpha$  subunits and three  $\beta$  subunits alternate.  $F_1$  contains three catalytic and three non-catalytic sites which bind adenine nucleotides. The catalytic sites are each  $\beta$  subunit at the interface with the adjacent  $\alpha$  subunit, whereas the non-catalytic sites are on each  $\alpha$  subunit at the interface with the adjacent  $\beta$  subunit [5]. During the ATP synthesis/hydrolysis, according to the “binding change model” [6], the conformational change in the  $(\alpha\beta)_3$  assembly occurs during the rotor rotation. During a  $360^\circ$  rotation the catalytic and non-catalytic site conformations change in TP (binding ATP), DP (binding ADP), and E (empty) conformations, driven by the rotation of the central stalk. The  $\beta$  subunits undergo a decrease in affinity for nucleotides with the sequential transition  $\beta_{TP} \rightarrow \beta_{DP} \rightarrow \beta_E$ , while the  $\alpha$  subunits only undergo the conformational changes during the rotor rotation. This mechanochemical mechanism of the  $F_1$  domain is driven by the  $H^+$  flow through  $F_0$  which generates the torsional movement. The  $H^+$  translocation from one side to the opposite side of the IMM within two asymmetrical half-channels on  $a$  subunit at the interface with the  $c$ -ring which hosts the  $H^+$  binding sites [7]. Differently from the bacterial enzyme, the mitochondrial  $F_0$  domain contains supernumerary subunits which intervene during the enzyme dimerization and oligomerization, which in turn play a morphological role in mitochondrial *crista* formation [8,9]. Moreover, the supernumerary subunits are important to form and open the permeability transition pore (PTP) inside the  $c$ -ring [10].

Accordingly, the IMM becomes permeable to solutes up to 1.5 kDa in a process defined permeability transition (PT) when the PTP, a  $Ca^{2+}$ -activated channel with high conductance, opens. It seems ascertained that the  $F_1F_0$ -ATPase is the main playmaker which triggers the PTP formation and opening. Additionally, a low conductance channel inhibited by both CsA and BKA could be formed by the adenine nucleotide translocase isoforms [11,12]. After about 50 years of debate, the arcane molecular mechanism of PTP was revealed by Sazanov’s group [10]. When  $Ca^{2+}$  concentration increases in the mitochondrial matrix, the  $F_1F_0$ -ATPase can replace the natural cofactor  $Mg^{2+}$  with  $Ca^{2+}$  on  $\beta$  subunits [13]. The  $Ca^{2+}$ -activated enzyme can sustain ATP hydrolysis [14]. Since  $Ca^{2+}$  has a larger atomic radius than  $Mg^{2+}$  it induces conformational changes in the  $F_1$  domain which are transmitted to the membrane-embedded subunits [15]. Under physiological and pathological conditions, according to the “bent-pull” model of the  $Ca^{2+}$ -activated  $F_1F_0$ -ATPase [16], the PTP opens within the  $c$ -ring. In detail, the lipid plug anchored to  $e$  subunit, a lyso-phosphatidylserine which penetrates and fills the hole of the  $c$ -ring at the intermembrane space, is pulled out by  $e$  subunit displacement. The different conformational states of the  $F_1F_0$ -ATPase when activated by  $Ca^{2+}$ , which apparently cannot occur when  $Mg^{2+}$  plays the cofactor role, permit the detachment of the  $F_1$  domain by pushing the phosphatidylserine that fills the hole at the matrix side when water molecules enter the  $c$ -ring [10]. The  $F_1F_0$ -ATPase activated by  $Ca^{2+}$  as cofactor undergoes conformational changes which open the PTP [17]. Since PTP opening leads to cell death [18] and PTP dysregulation is increasingly involved in severe human diseases [2], once identified the main macromolecular target responsible for PTP formation, several compounds have been considered and investigated as potential pore inhibitors [19].

The rare earth transition metals known as Lanthanides are widely used in medicine due to their physicochemical characteristics [20]. They play an increasingly recognized role in diagnosis and therapy,

other than being widely exploited in research. Gadolinium (Gd)-based compounds belonging to organometals are widely used in Magnetic Resonance Imaging (MRI) as a contrast medium [21] as well as putative anticancer drugs [22]. Although for clinical use Gd ion ( $Gd^{3+}$ ) is always chelated with specific ligands due to its high toxicity, it seems to accumulate in the tissues, especially in the brain, therefore its long-term use has raised emerging concern [23]. Interestingly, the trivalent  $Gd^{3+}$  has biophysical characteristics similar to the divalent  $Ca^{2+}$  (radius of  $Gd^{3+}$  1.05-1.11 Å vs  $Ca^{2+}$  1.00-1.06 Å), which allow it to replace  $Ca^{2+}$  in its biological and biochemical mechanisms. Accordingly, the biological effects are currently ascribed to the cationic form  $Gd^{3+}$ . Most likely,  $Gd^{3+}$  acts at the cellular level by directly interfering with the  $Ca^{2+}$  entry pathways.  $Gd^{3+}$  is also used in experimental tests as an inhibitor of  $Ca^{2+}$  channels activated by stretching [24]. The  $Gd^{3+}$ -based compounds used in MRI seem to have negative effects on the mitochondrial activity by altering ATP production, reducing mitochondrial oxidative capacities and also promoting cellular apoptosis [25] and other forms of cell death [26]. These effects were also related to the  $Gd^{3+}$  capability to promote PTP opening [27]. Conversely, the cation was also reported to act as a PTP blocker in mammalian mitochondria [16].

The possibility that  $Gd^{3+}$  may act on the mammalian  $F_1F_0$ -ATPase activated by  $Ca^{2+}$  differently from the  $Mg^{2+}$ -activated enzyme was investigated and compared with the effects on PTP opening. The results may not only contribute to casting light on some still unexplored molecular mechanisms of  $Gd^{3+}$  toxicity [26], but also may improve the knowledge on the mechanism of PTP formation and opening and broaden the spectrum of exogenous PTP modulators. Moreover, since membrane permeabilization often results in a cellular catastrophe and  $Gd^{3+}$  is widely employed in medical fields, such as research, diagnosis and therapy, the assessment of the  $Gd^{3+}$  action mechanism on the key enzyme in bioenergetics may be extremely useful to adequately exploit  $Gd^{3+}$  properties for medical purposes.

## 2. Materials and methods

### 2.1. Chemicals

Oligomycin (a mixture of oligomycins A, B and C), and Fura-FF were purchased from Vinci-Biochem (Vinci, Italy).  $Na_2ATP$  and gadolinium trichloride ( $GdCl_3$ ) were obtained from Sigma-Aldrich (Milan, Italy). Quartz double distilled water was used for all reagent solutions.

### 2.2. Preparation of the mitochondrial fractions

Swine hearts (*Sus scrofa domesticus*) were collected at a local abattoir and transported to the lab within 2 h in ice buckets at 0–4°C. After removal of fat and blood clots as much as possible, approximately 30–40 g of heart tissue was rinsed in ice-cold washing Tris-HCl buffer (medium A) consisting of 0.25 M sucrose, 10 mM Tris(hydroxymethyl)-aminomethane (Tris), pH 7.4 and finely chopped into fine pieces with scissors. Each preparation was made from one heart. Once rinsed, tissues were gently dried on blotting paper and weighted. Then tissues were homogenized in medium B consisting of 0.25 M sucrose, 10 mM Tris, 1 mM EDTA (free acid), 0.5 mg/ml BSA fatty acid free, pH 7.4 with HCl at a ratio of 10 ml medium B per 1 g of fresh tissue. After a preliminary gentle break up by Ultraturrax T25, the tissue was carefully homogenized by a motor-driven teflon pestle homogenizer (Braun Melsungen Type 853202) at 650 rpm with 3 up-and-down strokes. The mitochondrial fraction was then obtained by stepwise centrifugation (Sorvall RC2-B, rotor SS34). Briefly, the homogenate was centrifuged at 1,000xg for 5 min, thus yielding a supernatant and a pellet. The pellet was re-homogenized under the same conditions of the first homogenization and re-centrifuged at

1,000 $\times$ g for 5 min. The gathered supernatants from these two centrifugations, filtered through four cotton gauze layers, were centrifuged at 10,500 $\times$ g for 10 min to yield the raw mitochondrial pellet. The raw pellet was resuspended in medium A and further centrifuged at 10,500 $\times$ g for 10 min to obtain the final mitochondrial pellet. The latter was resuspended by gentle stirring using a Teflon Potter Elvehjem homogenizer in a small volume of medium A, thus obtaining a protein concentration of 30 mg/ml [28]. All steps were carried out at 0–4°C. The protein concentration was determined according to the colorimetric method of Bradford [29] by Bio-Rad Protein Assay kit II with BSA as standard. The mitochondrial preparations were then stored in liquid nitrogen until the evaluation of F<sub>1</sub>F<sub>0</sub>-ATPase activities.

### 2.3. Mitochondrial F-ATPase activity assays

Thawed mitochondrial preparations were immediately used for F-ATPase activity assays. The capability of ATP hydrolysis was assayed in a reaction medium (1 ml). The optimal conditions to obtain the maximal activity of the F<sub>1</sub>F<sub>0</sub>-ATPase, which depend on substrates concentration and pH values, are at 0.15 mg mitochondrial protein and 75 mM ethanolamine–HCl buffer pH 9.0, 6.0 mM Na<sub>2</sub>ATP and 2.0 mM MgCl<sub>2</sub> for the Mg<sup>2+</sup>-activated F<sub>1</sub>F<sub>0</sub>-ATPase assay, and 75 mM ethanolamine–HCl buffer pH 8.8, 3.0 mM Na<sub>2</sub>ATP and 2.0 mM CaCl<sub>2</sub> for the Ca<sup>2+</sup>-activated F<sub>1</sub>F<sub>0</sub>-ATPase assay [14,30]. These assay conditions were previously proven to elicit the maximal enzyme activities either stimulated by Mg<sup>2+</sup> or by Ca<sup>2+</sup> in swine heart mitochondria [31]. After 5 min preincubation at 37°C, the reaction, carried out at the same temperature, was started by the addition of the substrate Na<sub>2</sub>ATP and stopped after 5 min by the addition of 1 ml of ice-cold 15% (w/w) trichloroacetic acid (TCA) aqueous solution. Once the reaction was stopped, vials were centrifuged for 15 min at 3,500 rpm (Eppendorf Centrifuge 5202). In the supernatant, the concentration of inorganic phosphate (Pi) hydrolyzed by known amounts of mitochondrial protein, which is an indirect measure of F-ATPase activity, was spectrophotometrically evaluated [32]. According to the method employed, to detect the Pi release by the enzymatic reaction, the Pi released independently of the F<sub>1</sub>F<sub>0</sub>-ATPase activity should be quantified. To this aim, 1  $\mu$ l from a stock solution of 3 mg/ml oligomycin in dimethylsulfoxide was directly added to the reaction mixture before starting the reaction. The total ATPase activity was calculated by detecting the Pi in control tubes run in parallel and containing 1  $\mu$ l dimethylsulfoxide per ml reaction system. In each experimental set, control tubes were alternated to the condition to be tested. The employed dose of oligomycin, specific inhibitor of F-ATPases which selectively blocks the F<sub>0</sub> subunit ensured maximal enzyme activity inhibition and was currently used in F-ATPase assays [30].

To test the effect of Gd<sup>3+</sup> on the differently activated F<sub>1</sub>F<sub>0</sub>-ATPase activities, aqueous solutions of GdCl<sub>3</sub> at different standard concentrations were prepared immediately before each experimental set. Small aliquots (10  $\mu$ l) of these solutions were added to the reaction system and incubated at 37°C before starting the F<sub>1</sub>F<sub>0</sub>-ATPase reaction. Control tubes contained the same final volume, adjusted with 10  $\mu$ l of the reaction buffer.

In all experiments, the F<sub>1</sub>F<sub>0</sub>-ATPase activity was routinely measured by subtracting, from the Pi hydrolyzed by total ATPase activity, the Pi hydrolyzed in the presence of oligomycin [28]. In all experiments the F-ATPase activity, either activated by Ca<sup>2+</sup> as cofactor or by Mg<sup>2+</sup>, was expressed as  $\mu$ mol Pi·mg protein<sup>-1</sup>·min<sup>-1</sup>.

### 2.4. Kinetic analyses

The inhibition mechanism of Gd<sup>3+</sup> on the Ca<sup>2+</sup>- or Mg<sup>2+</sup>-activated F<sub>1</sub>F<sub>0</sub>-ATPases was explored by the graphical methods of Dixon and Cornish-Bowden plots, which complement one another. [33] To this aim, the 1/ $\nu$  (reciprocal of the enzyme activity  $\nu$ ) in Dixon plot or the S/ $\nu$  ratio in Cornish-Bowden plot were plotted as a

function of  $\text{GdCl}_3$  concentration. In all plots the enzyme specific activity was taken as the expression of  $v$ . To build these plots, different experimental sets were designed in which the  $\text{F}_1\text{F}_0$ -ATPase activity was evaluated in the presence of increasing  $\text{GdCl}_3$  concentrations at two ATP concentrations, keeping the divalent cofactor ( $\text{Mg}^{2+}$  or  $\text{Ca}^{2+}$ ) concentration constant. In these plots and in the definition of the binary or ternary complexes  $S$  indicates the ATP substrate. The values of  $K_i$ , which corresponds to the dissociation constant of the  $ES$  complex were calculated from the abscissa (changed to positive) of the intercept of the straight lines obtained in the Dixon plots. The values of  $K'_i$ , which represent the dissociation constant of the ternary  $ESI$  complex, were calculated as the abscissa (changed to positive) of the intercept of the straight lines obtained in the Cornish-Bowden plots.

The inactivation kinetics was investigated by incubating the mitochondrial suspensions in the presence of various  $\text{GdCl}_3$  concentrations (1.0 – 2.0 – 4.0 mM  $\text{GdCl}_3$  when the  $\text{F}_1\text{F}_0$ -ATPase was activated by  $\text{Mg}^{2+}$  as cofactor, and 1.0 – 1.5 – 2.0 mM  $\text{GdCl}_3$  when the  $\text{F}_1\text{F}_0$ -ATPase was activated by  $\text{Ca}^{2+}$ ). The  $\text{F}_1\text{F}_0$ -ATPase reaction activated by either  $\text{Mg}^{2+}$  or  $\text{Ca}^{2+}$  as cofactor was stopped after different time intervals (1-7 min) by 1 ml TCA 15% (w/w) addition. The pseudo first-order rate constants ( $k_{\text{obs}}$ ) for the enzyme inactivation were determined in both cases by plotting the natural logarithm of the residual activity vs time and extracting the rate constant from the slope [34].

A double-reciprocal plot is created by plotting the  $1/k_{\text{obs}}$  (x axis) as a function of the inverse of the  $\text{GdCl}_3$  concentrations ( $1/[\text{GdCl}_3]$ ) (y axis). The maximal inactivation rate ( $k_{\text{inact}}$ ) can be accurately determined and thus the inhibitor concentration at  $1/2k_{\text{inact}}$  ( $K_i$ ) can also be determined with accuracy because a straight line is formed. The y-intercept is  $1/k_{\text{inact}}$ , and the x-intercept is  $-1/K_i$ . The ratio  $k_{\text{inact}}/K_i$  is used to calculate the inhibitor efficiency, a rate constant for the potency of a mechanism-based inhibitor [35].

## 2.5. Evaluation of PTP

Immediately after the preparation of swine heart mitochondrial fractions, fresh mitochondrial suspensions (1mg/ml) were energized in the assay buffer (130 mM KCl, 1 mM  $\text{KH}_2\text{PO}_4$ , 20 mM HEPES, pH 7.2 with TRIS), incubated at 25°C with 1  $\mu\text{g}/\text{ml}$  rotenone and 5 mM succinate as respiratory substrate. To evaluate  $\text{Gd}^{3+}$  effect, selected  $\text{Gd}^{3+}$  concentrations, obtained by sampling small aliquots from standard  $\text{GdCl}_3$  aqueous solutions, as described in Section 2.3, were added to the mitochondrial suspensions before PTP evaluation. PTP opening was induced by the addition of low concentrations of  $\text{Ca}^{2+}$  (10  $\mu\text{M}$ ) as  $\text{CaCl}_2$  aqueous solution at fixed time intervals (1 min). The  $\text{Ca}^{2+}$  retention capacity (CRC), whose lowering indicates mPTP opening, was spectrofluorophotometrically evaluated in the presence of 0.8  $\mu\text{M}$  Fura-FF. The probe has different spectral properties in the absence and in the presence of  $\text{Ca}^{2+}$ , namely it displays excitation/emission spectra of 365/514 nm in the absence of  $\text{Ca}^{2+}$  (Fura-FF low  $\text{Ca}^{2+}$ ) and shifts to 339/507 nm in the presence of high  $\text{Ca}^{2+}$  concentrations (Fura-FF high  $\text{Ca}^{2+}$ ). PTP opening, was evaluated by the increase in the fluorescence intensity ratio (Fura-FF high  $\text{Ca}^{2+}$ )/(Fura-FF low  $\text{Ca}^{2+}$ ), which indicates a decrease in CRC [36]. All measurements were processed by LabSolutions RF software.

## 2.6. Calculations and statistics

The data represent the mean  $\pm$  SD (shown as vertical bars in the figures) of the number of experiments reported in the figure captions. In each experimental set, the analyses were carried out on different pools of animals. Statistical analyses were performed by SIGMASTAT software. The analysis of variance followed by Students–Newman–Keuls' test when F values indicated significance ( $P \leq 0.05$ ) was applied. Percentage data were *arcsin*-transformed before statistical analyses to ensure normality.



### 3. Results and discussion

The mPTP opening and the mitochondrial  $F_1F_0$ -ATPase participation in the mPTP are both linked to an abrupt  $Ca^{2+}$  increase in mitochondria. In detail, the substitution of the natural cofactor  $Mg^{2+}$  by  $Ca^{2+}$  as cofactor in the  $\beta$  subunits of the  $F_1F_0$ -ATPase [13] has been involved in the mechanism of mPTP formation [9,30]. The mitochondrial  $F_1F_0$ -ATPase can be activated by either  $Mg^{2+}$  or  $Ca^{2+}$ , which can both act as cofactor, even if by displaying different kinetic features [14,17]. The rare earth metal cation  $Gd^{3+}$ , whose effects on the mPTP are still partially known, offers the opportunity to verify the effect on the  $F_1F_0$ -ATPase and to explore its putative connection with the mPTP. Accordingly,  $Gd^{3+}$  was reported to induce mitochondrial dysfunction, probably due to PTP opening [27]. Acute toxicity of the intraperitoneally injected salt of all the stable rare earth compounds in mice at level of 300 to 500 mg/Kg were produced [37]. In erythrocyte membranes  $Gd^{3+}$ , which is able to interact with membrane phospholipids [38], would act as pore former [39]. Conversely,  $Gd^{3+}$  was shown to inhibit membrane permeabilization by physically modifying the membrane structure in a model system [40]. In this paper all the mitochondrial effects of  $Gd^{3+}$  were tested by adding selected concentrations of the chloride salt  $GdCl_3$  which in aqueous media dissociates yielding  $Gd^{3+}$  and  $Cl^-$ . We tried to exploit the  $Gd^{3+}$  inhibition mechanism to understand its modulatory role of  $Gd^{3+}$  on the  $Ca^{2+}$ -activated  $F_1F_0$ -ATPase when the PTP forms. So the observed effects are currently ascribed to  $Gd^{3+}$ , known to interact with proteins.

#### 3.1. $Gd^{3+}$ affects the $F_1F_0$ -ATPase activity either activated by $Mg^{2+}$ or by $Ca^{2+}$

The effect of  $GdCl_3$ , in the range of 0.01 – 5.0 mM, was evaluated on the  $F_1F_0$ -ATPase either activated by  $Mg^{2+}$  or by  $Ca^{2+}$  as cofactor (Fig. 2). Increasing  $GdCl_3$  concentrations promotes an exponential  $F_1F_0$ -ATPase activity decay independently of the divalent cofactors that sustain ATP hydrolysis. Both the differently activated  $F_1F_0$ -ATPase activities are increasingly inhibited by increasing  $GdCl_3$  concentrations. However, the main difference between the  $F_1F_0$ -ATPase activities when activated by  $Mg^{2+}$  or by  $Ca^{2+}$  as cofactor is that the  $F_1F_0$ -ATPase when activated by  $Mg^{2+}$  only attains a maximal 40% inhibition at the highest concentration tested (5mM  $GdCl_3$ ) (Fig. 2A), while when activated by  $Ca^{2+}$  the enzyme is progressively inhibited up to attain a value close to zero at 5 mM  $GdCl_3$  (Fig. 2B).

#### 3.2. The Inhibition mechanism is revealed by inhibition kinetics analyses

Kinetic studies, based on the building of Dixon and Cornish-Bowden plots, can lead to define the features of the enzyme–inhibitor complex in the presence or in the absence of the ATP substrate or cation cofactors. These kinetic analyses were carried out to understand the  $GdCl_3$  inhibition mechanism, most likely exerted by  $Gd^{3+}$ , on the  $F_1F_0$ -ATPase. The inhibition exerted by  $Gd^{3+}$  on the  $Mg^{2+}$ -activated  $F_1F_0$ -ATPase shows a competitive mechanism with respect to the ATP substrate (Fig. 3A,B) and an uncompetitive type mechanism with respect to the  $Mg^{2+}$  cofactor (Fig. 3C,D). The competitive inhibition indicates that the inhibitor only binds to the free enzyme, while the uncompetitive inhibition indicates that  $Gd^{3+}$  only binds to the enzyme- $Mg^{2+}$  complex. According to the mechanism of uncompetitive inhibition, usually observed when the enzyme has two or more binding sites [41],  $Gd^{3+}$  binds to a different site than that of the  $Mg^{2+}$  cofactor, but only when the enzyme–substrate (ES) complex is already formed, to yield the enzyme–substrate-inhibitor (ESI) complex.

The competitive inhibition mechanism is also exerted by  $Gd^{3+}$  on the  $Ca^{2+}$ -activated  $F_1F_0$ -ATPase with respect to the ATP substrate (Fig. 4A,B).  $Gd^{3+}$  blocks the ATP binding to the enzyme by inhibiting the ATPase activity irrespective of the cation cofactor. The  $K_i$  value of the  $F_1F_0$ -ATPase is about three times lower than that of

the  $\text{Mg}^{2+}$ -activated  $\text{F}_1\text{F}_0$ -ATPase ( $0.5 \pm 0.4$  mM vs  $1.4 \pm 0.1$  mM) (Table 1). These  $K_i$  values indicate that  $\text{Gd}^{3+}$  more efficiently competes with ATP in the substrate binding site to form the binary complex (*EI*) when the  $\text{F}_1\text{F}_0$ -ATPase is activated by  $\text{Ca}^{2+}$  as cofactor than when the enzyme is activated by  $\text{Mg}^{2+}$ . Moreover, when the natural cofactor  $\text{Mg}^{2+}$  is substituted by  $\text{Ca}^{2+}$ , the  $\text{F}_1\text{F}_0$ -ATPase undergoes a mixed type inhibition mechanism on the cofactor (Fig. 4C,D). This inhibition type indicates that the inhibitor  $\text{Gd}^{3+}$  can bind either to the free enzyme or to the enzyme  $\text{Ca}^{2+}$ -complex. These results prove that  $\text{Gd}^{3+}$  and  $\text{Ca}^{2+}$  bind to distinct enzyme sites. Since the  $\text{Gd}^{3+}$  binding site does not overlap with the  $\text{Ca}^{2+}$  binding site on  $\beta$  subunits [13], the  $\text{Ca}^{2+}$ -activated  $\text{F}_1\text{F}_0$ -ATPase can form either a binary (enzyme- $\text{Gd}^{3+}$ ) or a ternary ( $\text{Ca}^{2+}$ -enzyme- $\text{Gd}^{3+}$ ) complex with the inhibitor. However, on considering the dissociation constants of the enzyme-inhibitor complex ( $K_i$ ) and of the enzyme-substrate-inhibitor complex ( $K'_i$ ), since the  $K_i$  value is three times lower than the  $K'_i$  value, the formation of the binary complex (enzyme- $\text{Gd}^{3+}$ ) is preferred with respect to that of the ternary complex (enzyme-cofactor-inhibitor). Moreover, the  $K'_i$  values in the presence of  $\text{Mg}^{2+}$  or  $\text{Ca}^{2+}$  as cofactor are similar (Table 1), thus pointing out that the ternary complex is independent of the activating cation. In other words, even if  $\text{Gd}^{3+}$  preferentially binds to the enzyme before the cofactor binding to form the binary complex, it binds to the enzyme-cofactor complex to form the ternary complex with the same strength when the cofactor is  $\text{Mg}^{2+}$  or  $\text{Ca}^{2+}$ .

### 3.3. How the cofactor may affect the $\text{F}_1\text{F}_0$ -ATPase function

The different size of cations with a larger radius than  $\text{Mg}^{2+}$  ( $1.45$  Å) such as  $\text{Ca}^{2+}$  ( $1.94$  Å) would promote a different coordination chemistry in the catalytic sites of the  $\text{F}_1$  hexamer. The hypothesized more flexible coordination geometry, characterized by irregular bond distances and angles in the  $\beta$  subunits induced by  $\text{Ca}^{2+}$ , allows the accommodation of up to eight bonds while  $\text{Mg}^{2+}$  forms hexacoordinated octahedral complexes [42]. The nucleotide-binding to the catalytic and non-catalytic  $\text{F}_1\text{F}_0$ -ATPase subunits requires the coordination of the essential cofactor  $\text{Mg}^{2+}$  which contributes to yield the binding site asymmetry and generation of the different affinities for nucleotides [43]. The presence of  $\text{Ca}^{2+}$  as cofactor modifies the enzyme kinetic parameters [14] and ascribes to the  $\text{F}_1\text{F}_0$ -ATPase a new role in mitochondrial biology [9,17]. Indeed, the new cryo-EM structure of the  $\text{F}_1\text{F}_0$ -ATPase [10] highlights a thorough conformational change in the enzyme structure when the  $\text{Ca}^{2+}$  replaces  $\text{Mg}^{2+}$  in the catalytic site and triggers the PTP formation according to the “bent-pull” model of the *c*-ring-gated channel [16]. The role of  $\text{Ca}^{2+}$  in the catalytic sites of the enzyme is corroborated by mutagenesis studies carried out by Bernardi’s group [15]. Among the six bonds that coordinate the  $\text{Mg}^{2+}$  cofactor, only the  $\beta\text{Thr163}$  of P-loop is directly linked to the cation. The Thr-Ser substitution promotes a selective decrease in mitochondrial  $\text{Ca}^{2+}$ -ATPase hydrolysis of ATP [15,44] associated with a resistance to the  $\text{Ca}^{2+}$ -induced PTP opening [15].

The reduction in the  $\text{F}_1\text{F}_0$ -ATPase catalytic efficiency of upon exposure to  $\text{Gd}^{3+}$  helps to correlate the enzyme structure and function in a selected domain, and to understand the enzyme involvement in PTP formation. The natural logarithm of the residual activity (uninhibited rate minus inhibited rate) vs time provides the observed first-order rate constants calculated from the slopes of the straight lines obtained at different  $\text{GdCl}_3$  concentrations when either  $\text{Mg}^{2+}$  or  $\text{Ca}^{2+}$  act as cofactor of the  $\text{F}_1\text{F}_0$ -ATPase activity. The plots in Figure 5A and 6A show the typical time course of  $\text{Gd}^{3+}$ -mediated inhibition on the activity of the  $\text{F}_1\text{F}_0$ -ATPase when activated either by  $\text{Mg}^{2+}$  or by  $\text{Ca}^{2+}$  as cofactor, respectively. In both cases, the time course of the  $\text{Gd}^{3+}$ -mediated inhibition is well fitted to an exponential function. The  $k_{\text{obs}}$ , which is obtained from the slope of each straight line, displays a gradual  $\text{GdCl}_3$  concentration-dependent increase only when the  $\text{F}_1\text{F}_0$ -ATPase is activated by  $\text{Mg}^{2+}$  (Fig. 5A). The inhibition mechanism of  $\text{Gd}^{3+}$  on the  $\text{Mg}^{2+}$ - or the  $\text{Ca}^{2+}$ -activated  $\text{F}_1\text{F}_0$ -ATPase, depicted in figure 5B and figure 5B, respectively, shows the  $\text{GdCl}_3$  concentrations which promote the half-maximal enzyme inactivation in the presence of different cofactors. The  $\text{F}_1\text{F}_0$ -ATPase when activated by  $\text{Ca}^{2+}$

as cofactor shows a three times lower  $K_i$  value than when it is activated by  $Mg^{2+}$ -activated  $F_1F_0$ -ATPase (Table 1), suggesting that  $Gd^{3+}$  bound to the catalytic region affects the kinetics of cofactor-mediated ATP hydrolysis. The higher propensity of  $Gd^{3+}$  to react with the  $F_1F_0$ -ATPase when activated by  $Ca^{2+}$  than when activated by  $Mg^{2+}$  is also confirmed by a significantly higher  $k_{inact}$  value for the  $Ca^{2+}$ -activated  $F_1F_0$ -ATPase (Table 1). The inhibition potency of  $Gd^{3+}$ , which indicates the  $Gd^{3+}$  inhibition efficiency on the  $Mg^{2+}$ - and the  $Ca^{2+}$ -activated  $F_1F_0$ -ATPase, is shown by the  $k_{inact}/K_i$  ratio (Table 1).  $Gd^{3+}$  shows a  $k_{inact}/K_i$  ratio for the  $Ca^{2+}$ -activated  $F_1F_0$ -ATPase, which is 4.5 times higher than the ratio for the  $Mg^{2+}$ -activated  $F_1F_0$ -ATPase (Table 1). Therefore,  $Gd^{3+}$  more quickly reacts with the enzyme in the presence of  $Ca^{2+}$  as cofactor, resulting in a prompt and stronger inhibition of the  $F_1F_0$ -ATPase activity when activated by  $Ca^{2+}$  as cofactor. To sum up, all data indicate that when  $Ca^{2+}$  replaces the natural cofactor  $Mg^{2+}$  in the enzyme binding site, the  $F_1F_0$ -ATPase becomes more prone to the inhibition by  $Gd^{3+}$ .

### 3.4. PTP desensitization to $Ca^{2+}$

$Ca^{2+}$  pulses accumulate in the mitochondrial matrix and are released when the PTP opens. Mitochondria retain calcium and do not form the PTP until the IMM remains intact. The CRC, represents the capability of intact mitochondria to accumulate  $Ca^{2+}$ . According to the method adopted, the CRC decrease in  $GdCl_3$  treated mitochondria, revealed by an increase in fluorescence intensity, points out the  $Gd^{3+}$  ability to desensitize the PTP opening (Fig. 7A). In control mitochondria, the CRC decrease is revealed after 210 sec upon a two-train  $Ca^{2+}$  pulses, as shown by the rise in the (Fura-FF high  $Ca^{2+}$ )/(Fura-FF low  $Ca^{2+}$ ) ratio. Accordingly, the increase in CRC upon subsequent 10  $\mu M$   $Ca^{2+}$  additions at 1 min intervals, indicates that mitochondria in the presence of  $Gd^{3+}$  must attain a higher threshold value of  $Ca^{2+}$  concentration in the matrix to trigger PTP formation, with respect to control mitochondria. This phenomenon, known as PTP desensitization to  $Ca^{2+}$ , is shown by a delayed rise in the Fura-FF ratio, which indicates a decreased CRC (Fig. 7A). Consistently, the PTP formation extent, expressed as the ratio of the number of  $Ca^{2+}$  pulses required to induce the PTP in  $MgADP$  inhibited ( $CRC_i$ ) and untreated ( $CRC_o$ ) mitochondria [31], is doubled in the presence of 1.0 mM  $GdCl_3$  (Fig. 7B).

### 3.5. The $Gd^{3+}$ inhibition of the $F_1F_0$ -ATPase activity when $Ca^{2+}$ acts as cofactor is consistent with the PTP desensitization

We can speculate that the  $GdCl_3$  effects on the PTP are due to the interactions of  $Gd^{3+}$  in the  $F_1$  region of the  $F_1F_0$ -ATPase, which hamper the PTP formation. The  $GdCl_3$  preferential inhibition on the  $F_1F_0$ -ATPase when the cofactor is  $Ca^{2+}$  corroborates the link between the  $Ca^{2+}$ -activated  $F_1F_0$ -ATPase and the PTP and points out  $Gd^{3+}$  as a PTP inhibitor, consistently with other reports in swine mitochondria [44]. On the other hand, Lanthanide ions are long known as blockers of membrane permeabilization [40], even if this topic is still controversial [45]. Under the experimental conditions adopted, the strong binding of  $Gd^{3+}$  to the  $F_1F_0$ -ATPase catalytic domain when the enzyme activity is activated by  $Ca^{2+}$  hampers both ATP hydrolysis and PTP formation.

## 4. Conclusion

The results add further information on the mitochondrial effects of  $Gd^{3+}$ , which from a literature overview, are still controversial. Lanthanide ions including  $Gd^{3+}$  were shown to increase mitochondrial fluidity and to promote mitochondrial swelling and apoptosis in mice liver, thus strongly suggesting the induction of PTP opening [45].  $Gd^{3+}$  promoted PTP opening in rat liver mitochondria at 500  $\mu M$  concentration [27] and induced mitochondrial impairment and neuronal cell apoptosis [46]. On the contrary, recently  $Gd^{3+}$  was reported as

known PTP blocker in mammalian mitochondria [16]. These reports open intriguing questions on the PTP modulation by exogenous compounds. Most likely the  $Gd^{3+}$  effect and action mechanism on the membrane permeabilization mainly depend on the dose and on the experimental conditions. The concentration-dependent effects of  $Gd^{3+}$  on mitochondria were already pointed out [47].

On these bases, the mitochondrial membrane composition and the  $Gd^{3+}$  concentration may be crucial in determining the accessibility of  $Gd^{3+}$  to the  $F_1F_0$ -ATPase, especially on considering that  $Gd^{3+}$  by interacting with membrane phospholipids can modify the membrane structure [45].

The inhibition kinetic analyses confirm that in swine heart mitochondria the  $F_1F_0$ -ATPase is a molecular target of  $Gd^{3+}$  which directly interacts with the enzyme proteins. The  $Gd^{3+}$  effect on the  $F_1F_0$ -ATPase catalytic activity reinforces the link between PTP formation and the  $F_1F_0$ -ATPase activation in the presence of  $Ca^{2+}$  as cofactor. Indeed,  $Gd^{3+}$ , not only blocks PTP opening, but exerts a more efficient  $F_1F_0$ -ATPase inhibition when the natural  $Mg^{2+}$  cofactor is replaced by  $Ca^{2+}$ . Assuming that the enzyme has different conformations when it binds  $Mg^{2+}$  or  $Ca^{2+}$  [10] the molecular model that ascribes to  $Ca^{2+}$  insertion in the catalytic  $F_1F_0$ -ATPase sites the event which triggers the  $F_1F_0$ -ATPase conformational changes which open the PTP [9,15,17] is strongly corroborated. The role of  $Gd^{3+}$  as PTP blocker opens new perspectives in the putative protective role of this cation to prevent mitochondrial decay and cell death. Accordingly,  $GdCl_3$  administration to counteract ischemia/reperfusion injury was reported to attenuate the mitochondrial damage in liver cells [48] as well as cardiomyocyte apoptosis in rats [49].  $Gd^{3+}$  derivatives inhibited the mitochondrial pathway of apoptosis in human hepatocytes [50]. However, since the mitochondrial effects of  $Gd^{3+}$  are still poorly investigated, any extrapolation should be taken with caution and further studies are required.

## Acknowledgements

Danilo Matteuzzi and Roberto Giusti (Department of Veterinary Medical Sciences, University of Bologna) are gratefully acknowledged for kindly conferring swine hearts from a local abattoir to Biochemistry laboratories.

## Funding

This work was supported by a RFO grant from the University of Bologna, Italy.

## References

- [1] W. Junge, H. Sialaff, S. Engelbrecht, Torque generation and elastic power transmission in the rotary  $F(O)F(1)$ -ATPase, *Nature*. 459 (2009) 364–370. <https://doi.org/10.1038/nature08145>.
- [2] S. Nesci, F. Trombetti, A. Pagliarani, V. Ventrella, C. Algieri, G. Tioli, G. Lenaz, Molecular and Supramolecular Structure of the Mitochondrial Oxidative Phosphorylation System: Implications for Pathology, *Life*. 11 (2021) 242. <https://doi.org/10.3390/life11030242>.
- [3] W. Kühlbrandt, Structure and Mechanisms of F-Type ATP Synthases, *Annu. Rev. Biochem.* 88 (2019) 515–549. <https://doi.org/10.1146/annurev-biochem-013118-110903>.
- [4] S. Nesci, A. Pagliarani, C. Algieri, F. Trombetti, Mitochondrial F-type ATP synthase: multiple enzyme functions revealed by the membrane-embedded FO structure, *Crit. Rev. Biochem. Mol. Biol.* 55 (2020) 309–321. <https://doi.org/10.1080/10409238.2020.1784084>.
- [5] A. Hahn, K. Parey, M. Bublit, D.J. Mills, V. Zickermann, J. Vonck, W. Kühlbrandt, T. Meier, Structure of a Complete ATP Synthase Dimer Reveals the Molecular Basis of Inner Mitochondrial Membrane Morphology, *Mol. Cell*. 63 (2016) 445–456. <https://doi.org/10.1016/j.molcel.2016.05.037>.

- [6] P.D. Boyer, Catalytic site occupancy during ATP synthase catalysis, *FEBS Lett.* 512 (2002) 29–32. [https://doi.org/10.1016/S0014-5793\(02\)02293-7](https://doi.org/10.1016/S0014-5793(02)02293-7).
- [7] S. Nesci, F. Trombetti, V. Ventrella, A. Pagliarani, Opposite rotation directions in the synthesis and hydrolysis of ATP by the ATP synthase: hints from a subunit asymmetry, *J. Membr. Biol.* 248 (2015) 163–169. <https://doi.org/10.1007/s00232-014-9760-y>.
- [8] M. Strauss, G. Hofhaus, R.R. Schröder, W. Kühlbrandt, Dimer ribbons of ATP synthase shape the inner mitochondrial membrane, *EMBO J.* 27 (2008) 1154–1160. <https://doi.org/10.1038/emboj.2008.35>.
- [9] S. Nesci, A. Pagliarani, Incoming news on the F-type ATPase structure and functions in mammalian mitochondria, *BBA Advances.* 1 (2021) 100001. <https://doi.org/10.1016/j.bbadv.2020.100001>.
- [10] G. Pinke, L. Zhou, L.A. Sazanov, Cryo-EM structure of the entire mammalian F-type ATP synthase, *Nat Struct Mol Biol.* 27 (2020) 1077–1085. <https://doi.org/10.1038/s41594-020-0503-8>.
- [11] J. Karch, M.J. Bround, H. Khalil, M.A. Sargent, N. Latchman, N. Terada, P.M. Peixoto, J.D. Molkentin, Inhibition of mitochondrial permeability transition by deletion of the ANT family and CypD, *Sci Adv.* 5 (2019) eaaw4597. <https://doi.org/10.1126/sciadv.aaw4597>.
- [12] M.A. Neginskaya, M.E. Solesio, E.V. Berezhnaya, G.F. Amodeo, N. Mnatsakanyan, E.A. Jonas, E.V. Pavlov, ATP Synthase C-Subunit-Deficient Mitochondria Have a Small Cyclosporine A-Sensitive Channel, but Lack the Permeability Transition Pore, *Cell Rep.* 26 (2019) 11–17.e2. <https://doi.org/10.1016/j.celrep.2018.12.033>.
- [13] M.J. Hubbard, N.J. McHugh, Mitochondrial ATP synthase F1-beta-subunit is a calcium-binding protein, *FEBS Lett.* 391 (1996) 323–329.
- [14] S. Nesci, F. Trombetti, V. Ventrella, M. Pirini, A. Pagliarani, Kinetic properties of the mitochondrial F1FO-ATPase activity elicited by Ca(2+) in replacement of Mg(2+), *Biochimie.* 140 (2017) 73–81. <https://doi.org/10.1016/j.biochi.2017.06.013>.
- [15] V. Giorgio, V. Burchell, M. Schiavone, C. Bassot, G. Minervini, V. Petronilli, F. Argenton, M. Forte, S. Tosatto, G. Lippe, P. Bernardi, Ca(2+) binding to F-ATP synthase  $\beta$  subunit triggers the mitochondrial permeability transition, *EMBO Rep.* 18 (2017) 1065–1076. <https://doi.org/10.15252/embr.201643354>.
- [16] N. Mnatsakanyan, E.A. Jonas, ATP synthase c-subunit ring as the channel of mitochondrial permeability transition: Regulator of metabolism in development and degeneration, *J. Mol. Cell. Cardiol.* 144 (2020) 109–118. <https://doi.org/10.1016/j.yjmcc.2020.05.013>.
- [17] S. Nesci, A. Pagliarani, Ca<sup>2+</sup> as cofactor of the mitochondrial H<sup>+</sup>-translocating F1FO-ATP(hydrol)ase, *Proteins: Structure, Function, and Bioinformatics.* 89 (2021) 477–482. <https://doi.org/10.1002/prot.26040>.
- [18] T.M. Bauer, E. Murphy, Role of Mitochondrial Calcium and the Permeability Transition Pore in Regulating Cell Death, *Circ Res.* 126 (2020) 280–293. <https://doi.org/10.1161/CIRCRESAHA.119.316306>.
- [19] S. Nesci, The mitochondrial permeability transition pore in cell death: A promising drug binding bioarchitecture, *Medicinal Research Reviews.* 40 (2020) 811–817. <https://doi.org/10.1002/med.21635>.
- [20] G. Wang, Q. Peng, Y. Li, Lanthanide-Doped Nanocrystals: Synthesis, Optical-Magnetic Properties, and Applications, *Accounts of Chemical Research.* 44 (2011) 322–332. <https://doi.org/10.1021/ar100129p>.
- [21] G. Strijkers, W. M. Mulder, G. F. van Tilborg, K. Nicolay, MRI Contrast Agents: Current Status and Future Perspectives, *Anti-Cancer Agents in Medicinal Chemistry.* 7 (2007) 291–305. <https://doi.org/10.2174/187152007780618135>.
- [22] J. Chen, J. Ramos, M. Sirisawad, R. Miller, L. Naumovski, Motexafin gadolinium induces mitochondrially-mediated caspase-dependent apoptosis, *Apoptosis.* 10 (2005) 1131–1142. <https://doi.org/10.1007/s10495-005-0887-2>.
- [23] L. Pasquini, A. Napolitano, E. Visconti, D. Longo, A. Romano, P. Tomà, M.C.R. Espagnet, Gadolinium-Based Contrast Agent-Related Toxicities, *CNS Drugs.* 32 (2018) 229–240. <https://doi.org/10.1007/s40263-018-0500-1>.

- [24] L.C. Adding, G.L. Bannenberg, L.E. Gustafsson, Basic Experimental Studies and Clinical Aspects of Gadolinium Salts and Chelates, *Cardiovascular Drug Reviews*. 19 (2006) 41–56. <https://doi.org/10.1111/j.1527-3466.2001.tb00182.x>.
- [25] D.V. Bower, J.K. Richter, H. von Tengg-Kobligk, J.T. Heverhagen, V.M. Runge, Gadolinium-Based MRI Contrast Agents Induce Mitochondrial Toxicity and Cell Death in Human Neurons, and Toxicity Increases With Reduced Kinetic Stability of the Agent:, *Investigative Radiology*. 54 (2019) 453–463. <https://doi.org/10.1097/RLI.0000000000000567>.
- [26] M.J. Akhtar, M. Ahamed, H. Alhadlaq, S. Alrokayan, Toxicity Mechanism of Gadolinium Oxide Nanoparticles and Gadolinium Ions in Human Breast Cancer Cells, *Curr Drug Metab*. 20 (2019) 907–917. <https://doi.org/10.2174/1389200220666191105113754>.
- [27] J. Zhao, Z.-Q. Zhou, J.-C. Jin, L. Yuan, H. He, F.-L. Jiang, X.-G. Yang, J. Dai, Y. Liu, Mitochondrial dysfunction induced by different concentrations of gadolinium ion, *Chemosphere*. 100 (2014) 194–199. <https://doi.org/10.1016/j.chemosphere.2013.11.031>.
- [28] S. Nesci, V. Ventrella, F. Trombetti, M. Pirini, A. Pagliarani, The mitochondrial F1FO-ATPase desensitization to oligomycin by tributyltin is due to thiol oxidation, *Biochimie*. 97 (2014) 128–137. <https://doi.org/10.1016/j.biochi.2013.10.002>.
- [29] M.M. Bradford, A rapid and sensitive method for the quantitation of microgram quantities of protein utilizing the principle of protein-dye binding, *Anal. Biochem*. 72 (1976) 248–254. <https://doi.org/10.1006/abio.1976.9999>.
- [30] C. Algieri, F. Trombetti, A. Pagliarani, V. Ventrella, C. Bernardini, M. Fabbri, M. Forni, S. Nesci, Mitochondrial Ca<sup>2+</sup>-activated F1 FO -ATPase hydrolyzes ATP and promotes the permeability transition pore, *Ann. N. Y. Acad. Sci*. 1457 (2019) 142–157. <https://doi.org/10.1111/nyas.14218>.
- [31] C. Algieri, F. Trombetti, A. Pagliarani, V. Ventrella, S. Nesci, Phenylglyoxal inhibition of the mitochondrial F1FO-ATPase activated by Mg<sup>2+</sup> or by Ca<sup>2+</sup> provides clues on the mitochondrial permeability transition pore, *Arch. Biochem. Biophys*. 681 (2020) 108258. <https://doi.org/10.1016/j.abb.2020.108258>.
- [32] V. Ventrella, S. Nesci, F. Trombetti, P. Bandiera, M. Pirini, A.R. Borgatti, A. Pagliarani, Tributyltin inhibits the oligomycin-sensitive Mg-ATPase activity in *Mytilus galloprovincialis* digestive gland mitochondria, *Comp. Biochem. Physiol. C Toxicol. Pharmacol*. 153 (2011) 75–81. <https://doi.org/10.1016/j.cbpc.2010.08.007>.
- [33] A. Cornish-Bowden, A simple graphical method for determining the inhibition constants of mixed, uncompetitive and non-competitive inhibitors, *Biochem. J*. 137 (1974) 143–144.
- [34] V. Algieri, C. Algieri, L. Maiuolo, A. De Nino, A. Pagliarani, M.A. Tallarida, F. Trombetti, S. Nesci, 1,5-Disubstituted-1,2,3-triazoles as inhibitors of the mitochondrial Ca<sup>2+</sup>-activated F1 FO -ATP(hydrol)ase and the permeability transition pore, *Ann N Y Acad Sci*. 1485 (2021) 43–55. <https://doi.org/10.1111/nyas.14474>.
- [35] F. Ghanbari, K. Rowland-Yeo, J.C. Bloomer, S.E. Clarke, M.S. Lennard, G.T. Tucker, A. Rostami-Hodjegan, A critical evaluation of the experimental design of studies of mechanism based enzyme inhibition, with implications for in vitro-in vivo extrapolation, *Curr Drug Metab*. 7 (2006) 315–334. <https://doi.org/10.2174/138920006776359293>.
- [36] S. Nesci, C. Algieri, F. Trombetti, V. Ventrella, M. Fabbri, A. Pagliarani, Sulfide affects the mitochondrial respiration, the Ca<sup>2+</sup>-activated F1FO-ATPase activity and the permeability transition pore but does not change the Mg<sup>2+</sup>-activated F1FO-ATPase activity in swine heart mitochondria, *Pharmacol Res*. 166 (2021) 105495. <https://doi.org/10.1016/j.phrs.2021.105495>.
- [37] J.G. Graca, F.C. Davison, J.B. Feavel, Comparative toxicity of stable rare earth compounds. II. Effect of citrate and edetate complexing on acute toxicity in mice and guinea pigs, *Arch Environ Health*. 5 (1962) 437–444. <https://doi.org/10.1080/00039896.1962.10663310>.
- [38] null Ermakov YuA, A.Z. Averbakh, A.B. Arbuzova, S.I. Sukharev, Lipid and cell membranes in the presence of gadolinium and other ions with high affinity to lipids. 2. A dipole component of the boundary potential on membranes with different surface charge, *Membr Cell Biol*. 12 (1998) 411–426.

- [39] Y. Cheng, M. Liu, R. Li, C. Wang, C. Bai, K. Wang, Gadolinium induces domain and pore formation of human erythrocyte membrane: an atomic force microscopic study, *Biochim Biophys Acta*. 1421 (1999) 249–260. [https://doi.org/10.1016/s0005-2736\(99\)00125-x](https://doi.org/10.1016/s0005-2736(99)00125-x).
- [40] E.C. Gianulis, A.G. Pakhomov, Gadolinium modifies the cell membrane to inhibit permeabilization by nanosecond electric pulses, *Arch Biochem Biophys*. 570 (2015) 1–7. <https://doi.org/10.1016/j.abb.2015.02.013>.
- [41] I.H. Segel, Enzyme Kinetics, in: W.J. Lennarz, M.D. Lane (Eds.), *Encyclopedia of Biological Chemistry*, Academic Press, Waltham, 2013: pp. 216–220. <https://doi.org/10.1016/B978-0-12-378630-2.00012-8>.
- [42] R. Casadio, B.A. Melandri, CaATP inhibition of the MgATP-dependent proton pump (H<sup>+</sup>-ATPase) in bacterial photosynthetic membranes with a mechanism of alternative substrate inhibition, *JBIC*. 1 (1996) 284–291. <https://doi.org/10.1007/s007750050055>.
- [43] W.D. Frasch, The participation of metals in the mechanism of the F<sub>1</sub>-ATPase, *Biochim. Biophys. Acta*. 1458 (2000) 310–325.
- [44] L. Nathanson, Z. Gromet-Elhanan, Mutations in the  $\beta$ -subunit Thr159 and Glu184 of the *Rhodospirillum rubrum* FOF1 ATP synthase reveal differences in ligands for the coupled Mg<sup>2+</sup>- and decoupled Ca<sup>2+</sup>-dependent FOF1 activities, *Journal of Biological Chemistry*. 275 (2000) 901–905. <https://doi.org/10.1074/jbc.275.2.901>.
- [45] H. Liu, L. Yuan, X. Yang, K. Wang, La(3+), Gd(3+) and Yb(3+) induced changes in mitochondrial structure, membrane permeability, cytochrome c release and intracellular ROS level, *Chem Biol Interact*. 146 (2003) 27–37. [https://doi.org/10.1016/s0009-2797\(03\)00072-3](https://doi.org/10.1016/s0009-2797(03)00072-3).
- [46] X. Feng, Q. Xia, L. Yuan, X. Yang, K. Wang, Impaired mitochondrial function and oxidative stress in rat cortical neurons: implications for gadolinium-induced neurotoxicity, *Neurotoxicology*. 31 (2010) 391–398. <https://doi.org/10.1016/j.neuro.2010.04.003>.
- [47] J. Zhao, L. Ma, X. Xiang, Q.-L. Guo, F.-L. Jiang, Y. Liu, Microcalorimetric studies on the energy release of isolated rat mitochondria under different concentrations of gadolinium (III), *Chemosphere*. 153 (2016) 414–418. <https://doi.org/10.1016/j.chemosphere.2016.03.082>.
- [48] W.-H. Zhang, J.-S. Wang, Y. Zhou, J.-Y. Li, Gadolinium chloride and salvia miltiorrhiza compound ameliorate reperfusion injury in hepatocellular mitochondria, *World J Gastroenterol*. 9 (2003) 2040–2044. <https://doi.org/10.3748/wjg.v9.i9.2040>.
- [49] M. Chen, Y. Zheng, Y. Song, J. Xue, Z. Liang, X. Yan, D. Luo, Pretreatment with low-dose gadolinium chloride attenuates myocardial ischemia/reperfusion injury in rats, *Acta Pharmacol Sin*. 37 (2016) 453–462. <https://doi.org/10.1038/aps.2015.156>.
- [50] T. Yu, M. Zhen, J. Li, Y. Zhou, H. Ma, W. Jia, C. Wang, Anti-apoptosis effect of amino acid modified gadofullerene via a mitochondria mediated pathway, *Dalton Trans*. 48 (2019) 7884–7890. <https://doi.org/10.1039/c9dt00800d>.

## Figure captions

Figure 1. Subunit composition of mammalian mitochondrial F<sub>1</sub>F<sub>0</sub>-ATPase. The enzyme subunits are drawn as ribbon representations obtained from modified PDB ID code: 6TT7. The letter colors are the same as those of the subunits to which the structures belong.

Figure 2. Dose-response curve of GdCl<sub>3</sub> inhibition of the F<sub>1</sub>F<sub>0</sub>-ATPase activity. A) F<sub>1</sub>F<sub>0</sub>-ATPase activated by Mg<sup>2+</sup> (Mg<sup>2+</sup>-activated F<sub>1</sub>F<sub>0</sub>-ATPase) (□) and by Ca<sup>2+</sup> (Ca<sup>2+</sup>-activated F<sub>1</sub>F<sub>0</sub>-ATPase) (○) activities in the presence of increasing GdCl<sub>3</sub> concentrations. Data represent the mean  $\pm$  SD from three independent experiments carried out on different mitochondrial preparations.

Figure 3. Inhibition kinetics of the mitochondrial  $Mg^{2+}$ -activated  $F_1F_0$ -ATPase by  $GdCl_3$ . Dixon (A, C) and Cornish–Bowden (B, D) plots at 2mM  $MgCl_2$  plus 3 mM (○) or 6 mM (●) ATP (A,B); at 6 mM ATP plus 0.5 mM (□) or 2 mM (■)  $Mg^{2+}$  (C, D). The experimental design to build these plots is detailed in Section 2.4. All points represent the mean  $\pm$  SD (vertical bars) of four distinct experiments carried out on different mitochondrial preparations.

Figure 4. Inhibition kinetics of the mitochondrial  $Ca^{2+}$ -activated  $F_1F_0$ -ATPase by  $GdCl_3$ . Dixon (A, C) and Cornish–Bowden (B, D) plots at 2mM  $CaCl_2$  plus 1 mM (○) or 3 mM (●) ATP (A,B); at 3 mM ATP plus 0.5 mM (□) or 2 mM (■)  $Ca^{2+}$  (C, D). The experimental design to build these plots is detailed in Section 2.4. All points represent the mean  $\pm$  SD (vertical bars) of four distinct experiments carried out on different mitochondrial preparations.

Figure 5. Inactivation kinetics of the  $Mg^{2+}$ -activated  $F_1F_0$ -ATPase by increasing  $GdCl_3$  concentrations. (A) Semilogarithmic plot of the residual activity ( $\Theta$ ) *versus* time at fixed concentrations of  $GdCl_3$  ( $\Delta$ ) 1.0 mM, ( $\diamond$ ) 2.0 mM, ( $\square$ ) 4.0 mM. (B) Replot of the reciprocal of first-order rate constant ( $k_{obs}$ ) from the straight lines of (A). Each point corresponds to  $GdCl_3$  ( $\blacktriangle$ ) 1.0 mM, ( $\blacklozenge$ ) 2.0 mM, and ( $\blacksquare$ ) 4.0 mM. The experimental design to build these plots is detailed in Section 2.4. All points represent the mean  $\pm$  SD (vertical bars) of four distinct experiments carried out on different mitochondrial preparations.

Figure 6. Inactivation kinetics of the  $Ca^{2+}$ -activated  $F_1F_0$ -ATPase by increasing  $GdCl_3$  concentrations. (A) Semilogarithmic plot of the residual activity ( $\Theta$ ) *versus* time at fixed concentrations of  $GdCl_3$  (○) 1.0 mM, (□) 1.5 mM, (□) 2.0 mM. (B) Replot of the reciprocal of first-order rate constant ( $k_{obs}$ ) from the straight lines of (A). Each point corresponds to 1.0 mM  $GdCl_3$  (●) 1.5 mM  $GdCl_3$  (■) and 2 mM ( $\blacktriangle$ ). The experiments were carried out as detailed in Section 2.4. All points represent the mean  $\pm$  SD (vertical bars) of four distinct experiments carried out on different mitochondrial preparations.

Figure 7. Evaluation of mPTP opening. Representative curves (A) of the calcium retention capacity (CRC). CRC was monitored in response to subsequent 10  $\mu$ M  $CaCl_2$  pulses (shown by the arrows), as detailed in the Section 2.5, in the absence (Control-black line) and in the presence of the inhibitors 2 mM MgADP (red line), and 1 mM  $GdCl_3$  (green line). B) Quantitation of the mPTP displayed as the ratio of the number of calcium pulses required to induce the mPTP opening in MgADP-inhibited ( $CRC_i$ ) and uninhibited ( $CRC_o$ ) mitochondria. Data represent the mean  $\pm$  SD from three independent experiments carried out on distinct mitochondrial preparations. \* indicates significant differences with respect to the control ( $P \leq 0.05$ ).



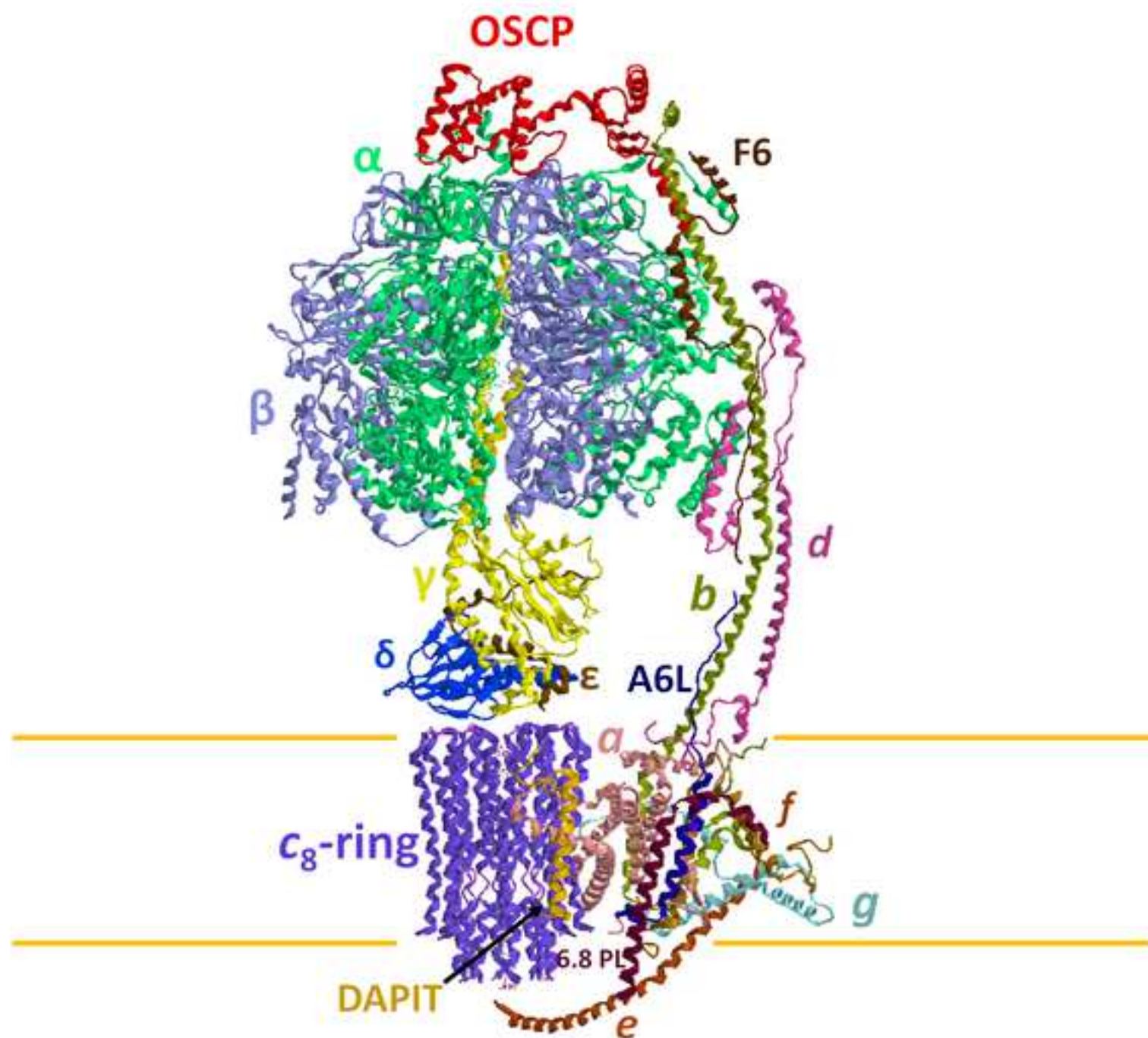


Figure 2

[Click here to access/download;Figure;Figure 2.tif](#)

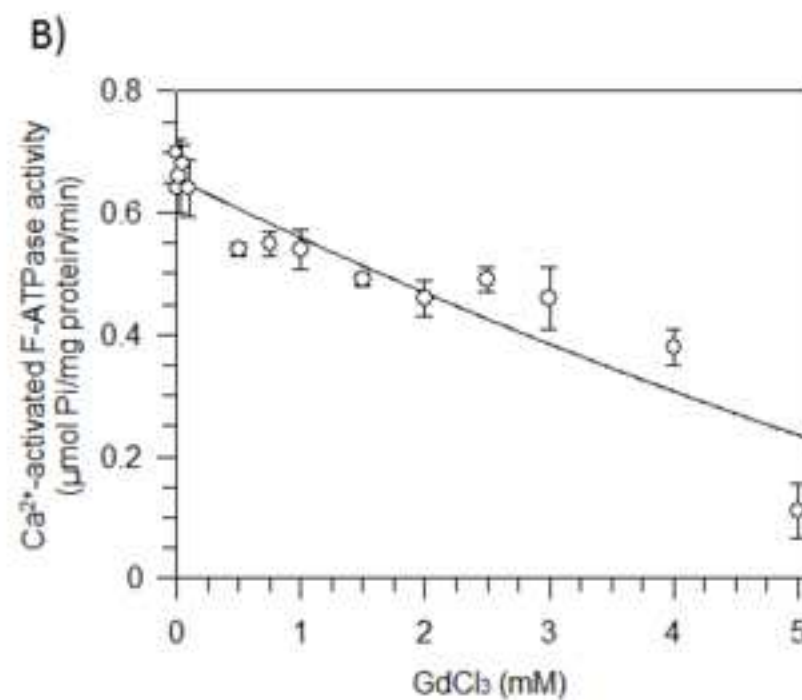
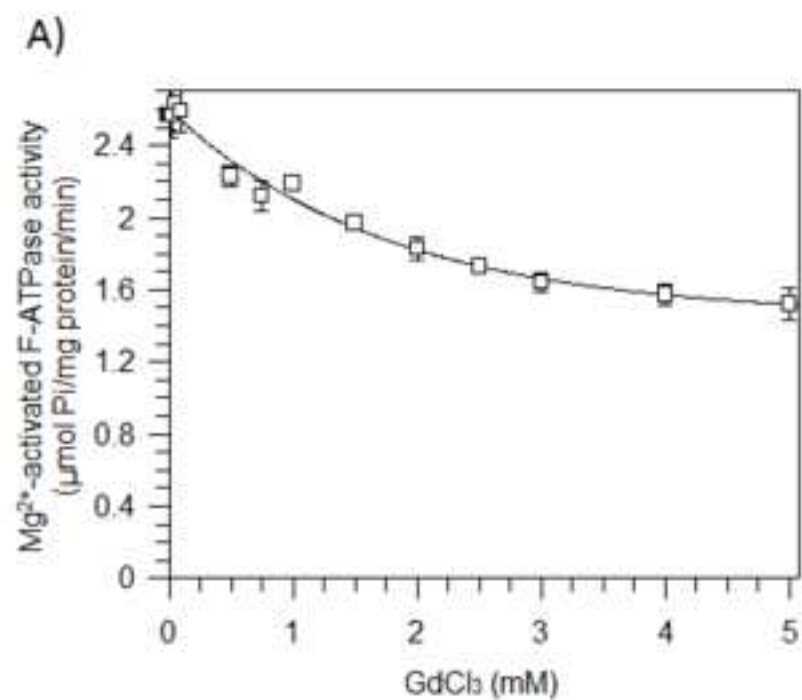


Figure 3

[Click here to access/download;Figure;Figure 3.tif](#)

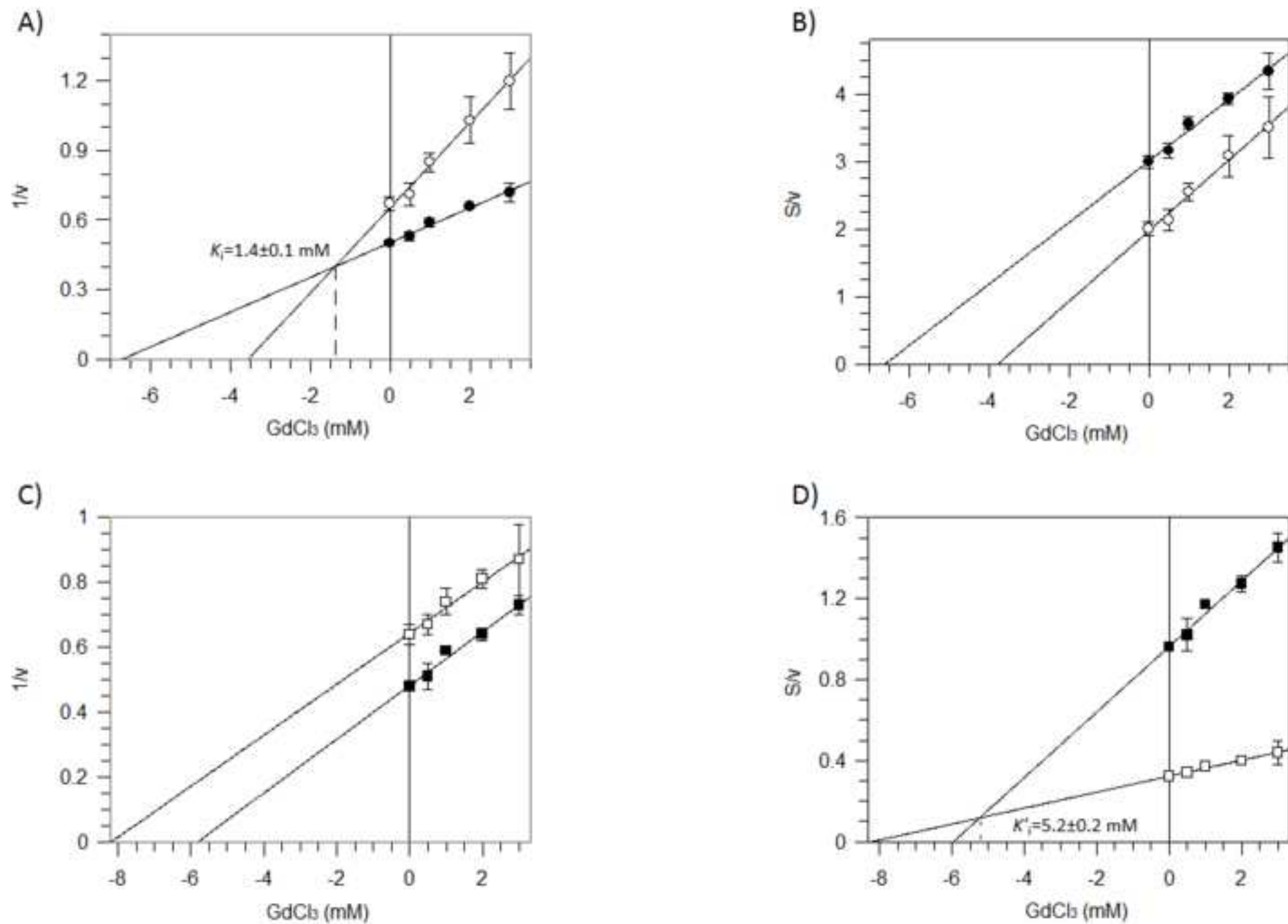


Figure 4

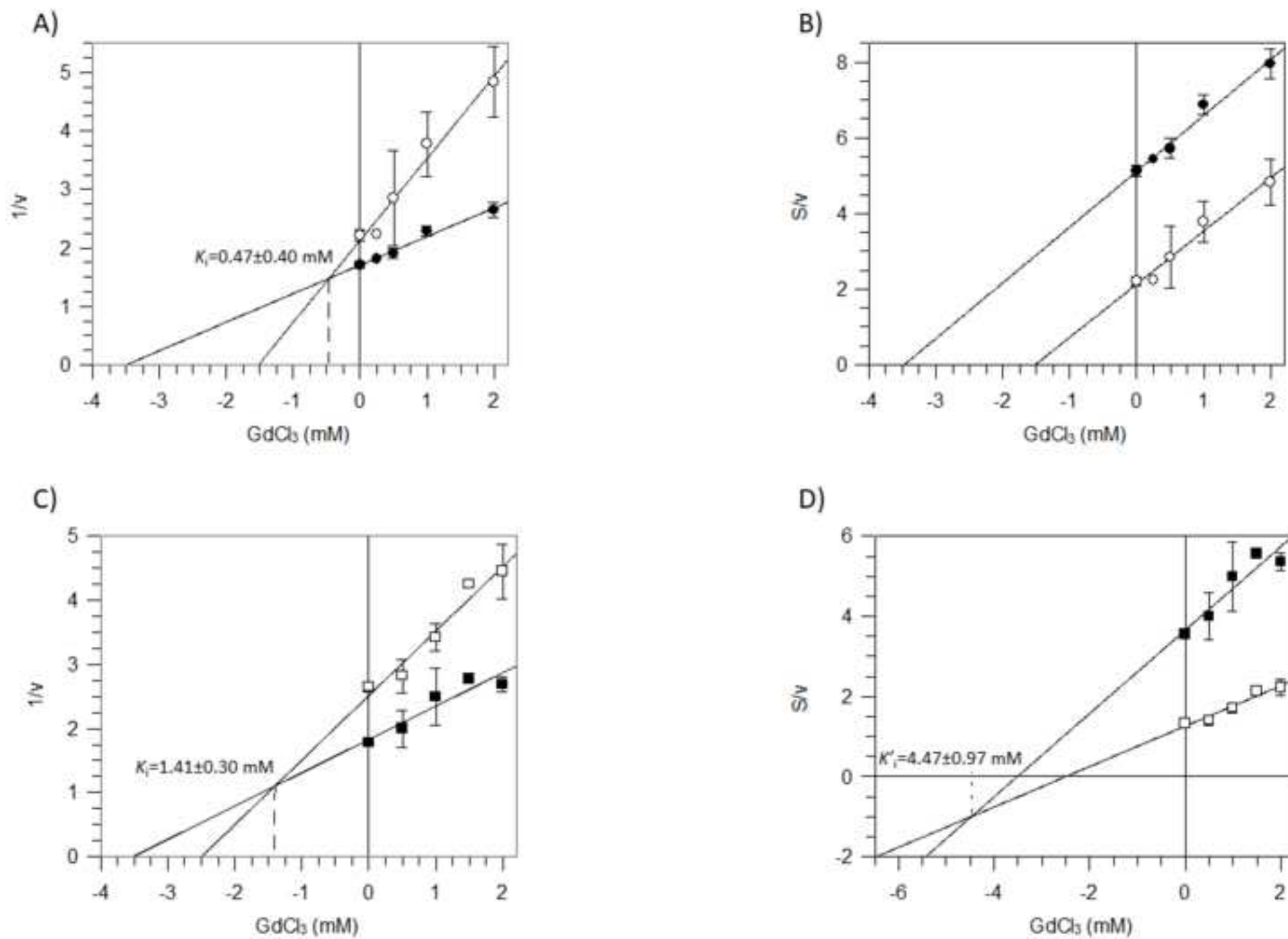


Figure 5

[Click here to access/download;Figure;Figure 5.tif](#)

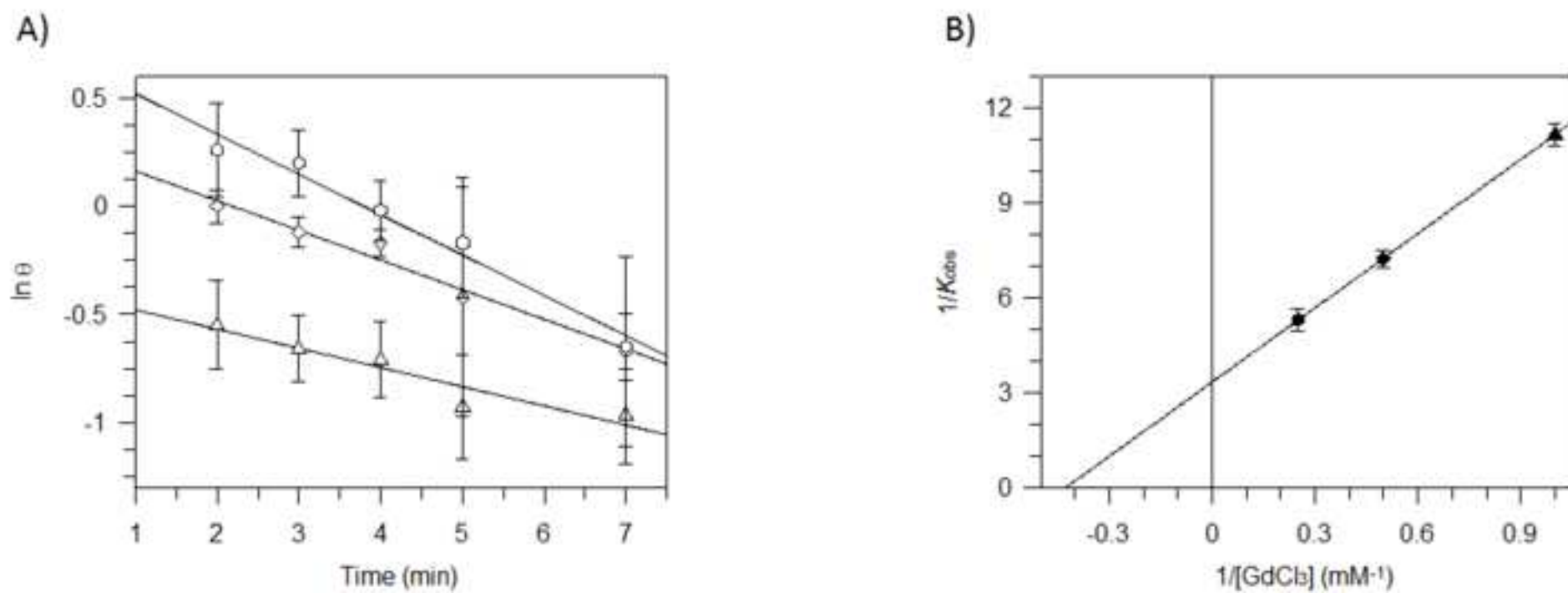
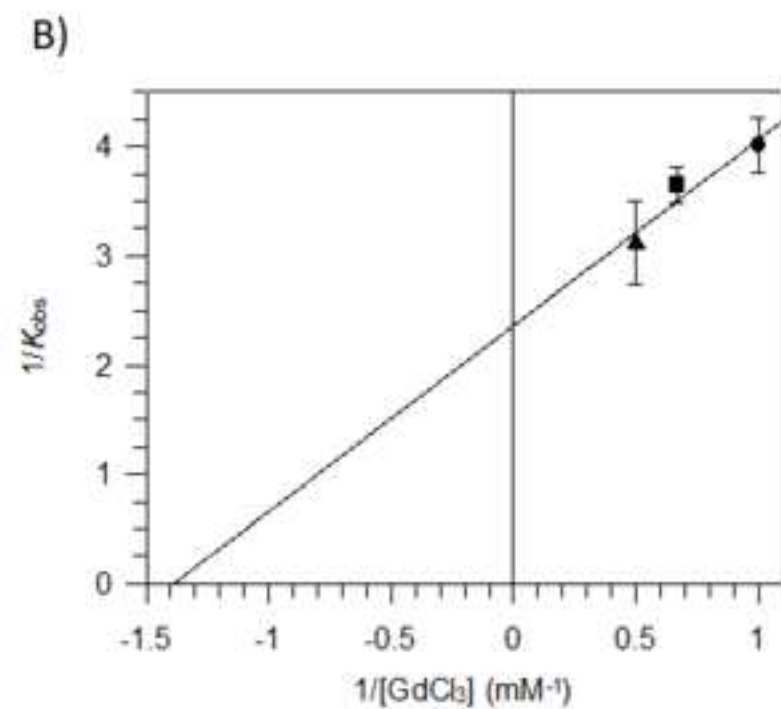
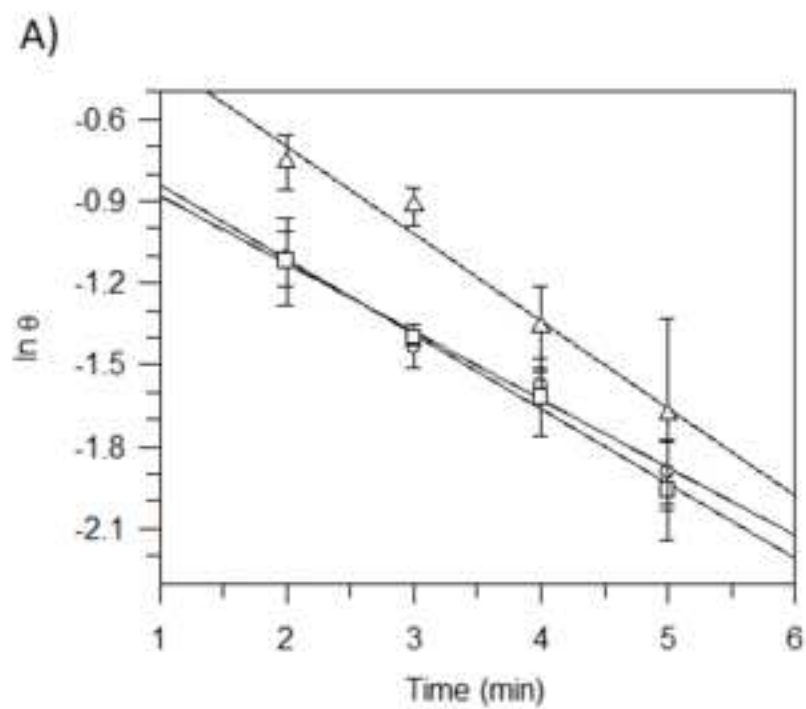


Figure 6

[Click here to access/download;Figure;Figure 6.tif](#)



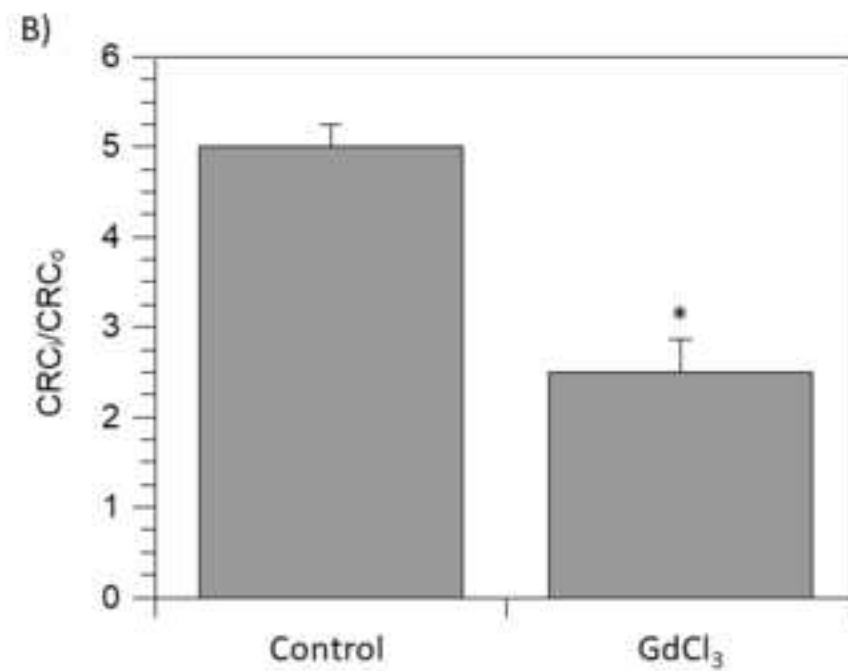
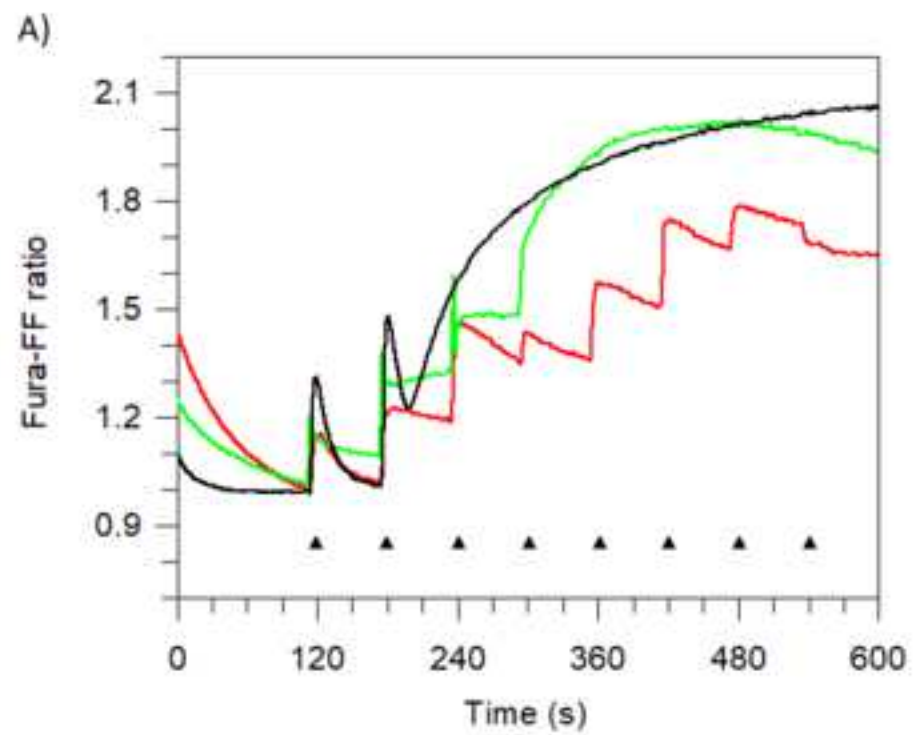


Table 1

Kinetic constants of  $Gd^{3+}$  inhibition on the  $F_1F_0$ -ATPase activated by the cofactors  $Mg^{2+}$  or  $Ca^{2+}$ .

	ATP substrate		Cofactor		$K_i$ (mM)	$k_{inact}$ (s <sup>-1</sup> )	$k_{inact}/K_i$ (mM <sup>-1</sup> ·s <sup>-1</sup> )
	$K_i$ (mM)	$K'_i$ (mM)	$K_i$ (mM)	$K'_i$ (mM)			
$Mg^{2+}$ -ATPase	1.4±0.1A	∞	∞	5.2±0.2A	2.35±0.35A	0.30±0.04A	0.13±0.02A
$Ca^{2+}$ -ATPase	0.5±0.4B	∞	1.4±0.3a	4.5±1.0Ab	0.72±0.11B	0.42±0.06B	0.59±0.09B

$F_1F_0$ -ATPase activated by  $Mg^{2+}$  ( $Mg^{2+}$ -ATPase);  $F_1F_0$ -ATPase activated by  $Ca^{2+}$  ( $Ca^{2+}$ -ATPase); Substrate (ATP); Cofactor ( $Mg^{2+}$  or  $Ca^{2+}$ ).  $K_i$  and  $K'_i$  values were graphically obtained from the Dixon and Cornish Bowden plots, respectively reported in Fig. 3 for  $Mg^{2+}$ -activated  $F_1F_0$ -ATPase and in Fig. 5 for the  $Ca^{2+}$ -activated  $F_1F_0$ -ATPase.  $K_i$  and  $k_{inact}$  values of  $Mg^{2+}$ -activated  $F_1F_0$ -ATPase or  $Ca^{2+}$ -activated  $F_1F_0$ -ATPase were graphically obtained from the double reciprocal plots of Fig. 4B and Fig. 5B, respectively. Details are reported in the section 2.4. Data are the mean ± SD of three different experiments carried out on distinct mitochondrial pools. Different upper case letters indicate significantly different values ( $P \leq 0.05$ ) between different activated  $F_1F_0$ -ATPases; different lower case letters indicate different values ( $P \leq 0.05$ ) within the same treatment. ∞= not detectable.



## Author Statement

CA, investigation and methodology; FT and AP, writing - review & editing; MF, resources; AP and SN, visualization; FT, AP and SN, validation; SN, supervision and writing origina draft.